Journal of Solid State Chemistry **164,** 201–209 (2002)
doi:10.1006/jssc.2001.9460, available online at http://www.idealibrary.com on IDEAL®

Magnetic and Electrical Properties, ^{151}Eu Mössbauer Spectroscopy, and Chemical Bonding of *RE*AgMg (*RE* = La, Ce, Eu, Yb) and EuAuMg

Dirk Johrendt,* Gunter Kotzyba,† Henning Trill,‡ Bernd D. Mosel,‡ Hellmut Eckert,‡ Thomas Fickenscher,† and Rainer Pöttgen†

*Institut für Anorganische Chemie und Strukturchemie II, Heinrich-Heine-Universität Düsseldorf, Universitätsstraße 1, D-40225 Düsseldorf, Germany; †Department Chemie, Ludwig-Maximilians-Universität München, Butenandtstraße 5-13 (Haus D), D-81377 Munich, Germany; and ‡Institut für Physikalische Chemie, Universität Münster, Schloßplatz 4/7, D-48149 Münster, Germany

E-mail: johrendt@uni-duesseldorf.de; pottgen@uni-muenster.de; eckerth@uni-muenster.de.

Received August 7, 2001; in revised form November 1, 2001; accepted November 16, 2001

Single-phase samples of *RE*AgMg (*RE* = La, Ce, Eu, Yb) and EuAuMg were prepared by reacting the elements in sealed tantalum tubes in a high-frequency furnace. LaAgMg and CeAgMg adopt the hexagonal ZrNiAl-type structure, while EuAgMg, YbAgMg, and EuAuMg crystallize with the orthorhombic TiNiSi type. Chemical bonding was exemplarily investigated for EuAgMg and EuAuMg on the basis of TB-LMTO-ASA calculations. Magnetic susceptibility measurements indicate Pauli paramagnetism for LaAgMg and YbAgMg with room-temperature susceptibilities of $2.4(1)\times10^{-9}$ and $1.5(1)\times10^{-9}$ m^3/mol, respectively. CeAgMg remains paramagnetic down to 2 K. The experimental magnetic moment of 2.52(2) μ_B/Ce above 50 K is compatible with trivalent cerium. EuAgMg and EuAuMg are paramagnetic above 50 K with experimental magnetic moments of 7.99(5) μ_B/Eu for the silver and 7.80(5) μ_B/Eu for the gold compound, indicating divalent europium. Ferromagnetic ordering is detected at T_C = 22.0(3) K (EuAgMg) and T_C = 36.5(5) K (EuAuMg). At 4.2 K and 5 T the saturation magnetizations are 7.1(1) and 7.3(1) μ_B/Eu for EuAgMg and EuAuMg, respectively. According to the very small hysteresis, EuAgMg and EuAuMg may be classified as soft ferromagnets. All compounds are metallic conductors. For EuAgMg and EuAuMg freezing of spin-disorder scattering is observed below T_C. At 78 K ^{151}Eu Mössbauer spectra show isomer shifts of −9.00(4) and −8.72(8) mm/s for EuAgMg and EuAuMg, respectively. Full magnetic hyperfine field splitting is detected at 4.2 K with hyperfine fields of 17.4(1) and 18.3(2) T at the europium nuclei of EuAgMg and EuAuMg.

Key Words: **magnetism; mössbauer spectroscopy; electronic structure.**

INTRODUCTION

The structures of the equiatomic intermetallic *RET*Mg (*RE* = rare-earth element; *T* = Pd, Ag, Au) and *RET*Cd (*T* = Cu, Pd, Au) compounds have recently been studied and some physical properties were reported (1–8). These intermetallics crystallize with the hexagonal ZrNiAl structure (9–11) in the case of trivalent rare-earth metals and with the orthorhombic TiNiSi type (12) when the rare-earth element is divalent, i.e., europium and ytterbium.

First magnetic investigations of these materials revealed a nonmagnetic ground state for YbAuMg and YbAuCd (6), while ferromagnetic ordering is detected at 28 and 62 K in EuAuCd (6) and GdPdCd (7). CePdMg (3) contains stable trivalent cerium; however, no magnetic ordering is evident down to 2 K.

We have now extended our structure–property investigations of the *RET*Mg intermetallics with respect to the silver-containing compounds. Herein, we report on susceptibility and resistivity measurements on LaAgMg, CeAgMg, EuAgMg, YbAgMg, and the related gold compound EuAuMg. For both europium compounds we also studied the magnetic hyperfine interactions by ^{151}Eu Mössbauer spectroscopy and we investigated the chemical bonding by TB-LMTO-ASA band structure calculations.

EXPERIMENTAL

Synthesis

All samples were prepared from the elemental components by reactions in sealed tantalum tubes in a high-frequency furnace as described previously (8). The compounds were obtained in amounts of about 1 g. The purity of the samples was checked by X-ray powder diffractograms (Stoe Stadi P) using Cu$K\alpha_1$ radiation and silicon (a = 543.07 pm) as an external standard. The experimental patterns were compared with theoretical ones which were calculated with the LAZY-PULVERIX program (13).

Physical Property Measurements

The magnetic susceptibilities were determined with a MPMS *XL* SQUID magnetometer (Quantum Design, Inc.)

0022-4596/02 $35.00

in the temperature range 2 to 300 K with magnetic flux densities up to 5 T. Resistivity measurements were performed on polycrystalline pieces (edges up to 2 mm) of LaAgMg, CeAgMg, EuAgMg, YbAgMg, and EuAuMg using a four-probe technique. A constant current (Keithley Source Meter 2400) was applied to the sample and the resulting voltage was measured with a Keithley nanovoltmeter 2182. The four copper contacts were glued to the samples with a well-conducting silver paste. The samples were fixed on a closed-cycle cooling system (Cryodyne 22 CP, CTI-Cyrogenics) using a low-temperature paste (Cryophysics, 7031 insulating varnish and adhesive). The temperature was controlled by a silicon diode (Lake Shore, model 330) between 8 and 320 K with an accuracy better than ± 0.1 K. In each measurement the temperature was varied up and down in steps of 2 K. Since the polycrystalline pieces had quite irregular shapes, we could only determine the temperature dependence of the resistivity. Specific resistivities could not be determined reliably.

^{151}Eu Mössbauer Spectroscopy

The 21.53 keV transition of ^{151}Eu with an activity of 130 MBq (2% of the total activity of a ^{151}Sm:EuF_3 source) was used for the Mössbauer spectroscopic experiments. The measurements were performed with a commercial helium bath cryostat. The temperature of the absorber could be varied from 4.2 to 300 K and was measured with a metallic resistance thermometer with a precision better than ± 0.5 K. The source was kept at room temperature. The material for the Mössbauer spectroscopic investigation was the same as for the susceptibility measurements. The sample was diluted with sugar and placed within a thin-walled PVC container at a thickness corresponding to about 10 mg of Eu/cm^2.

Electronic Structure Calculations

Self-consistent band structure calculations were exemplarily performed for EuAgMg and EuAuMg using the LMTO method in its scalar-relativistic version (program TB-LMTO-ASA (14)). A detailed description may be found elsewhere (15, 16). Reciprocal space integrations were performed with the tetrahedron method using 105 k-points within the irreducible wedge of the Brillouin zone (17). The basis sets consisted of 6*s*/6*p*/5*d*/4*f* for Eu, 5*s*/5*p*/4*d*/4*f* for Ag, and 3*s*/3*p*/3*d* for Mg. The 6*p* orbitals of Eu, 4*f* of Ag, and 3*d* of Mg were treated by the down-folding technique (18). To achieve space filling within the atomic sphere approximation, interstitial spheres are introduced to avoid too large overlap of the atom-centered spheres. The empty spheres positions and radii were calculated automatically. We did not allow overlaps of more than 15% for any two atom centered spheres. Owing to the magnetic properties of the Eu 4*f* shell, spin-polarized calculations were performed using the exchange-correlation potential by Barth and Hedin (19). The COHP (*C*rystal *O*rbital *H*amilton *P*opulation) method was used for the bond analysis (20). COHP gives the energy contributions of all electronic states for a selected bond. The values are negative for bonding and positive for antibonding interactions. With respect to the well-known COOP diagrams, we plot COHP(E) to obtain positive values for bonding states.

RESULTS AND DISCUSSION

Crystal Chemistry and Chemical Bonding

LaAgMg and CeAgMg crystallize with the ZrNiAl-type structure (9–11). As an example, we present a projection of the CeAgMg structure in Fig. 1. The silver atoms adopt two crystallographically different sites Ag1 and Ag2. The Ag1 atoms have a trigonal prismatic coordination of cerium atoms, while the Ag2 atoms have six magnesium neighbors in the same arrangement. These [Ag1Ce$_6$] and [Ag2Mg$_6$] prisms are capped by three magnesium and cerium atoms, respectively. Apart from this purely geometrical description, we can descibe the CeAgMg structure by a three-dimensional [AgMg] network in which the cerium atoms are located in distorted hexagonal channels. For a more detailed description we refer to our previous work (8).

EuAgMg, EuAuMg, and YbAgMg adopt the orthorhombic TiNiSi type (12). An examplary view of the EuAuMg structure approximately along the *y* axis is displayed in Fig. 2. The gold and magnesium atoms form a three-dimensional network of strongly puckered and orthorhombically distorted Au_3Mg_3 hexagons. The Au–Mg

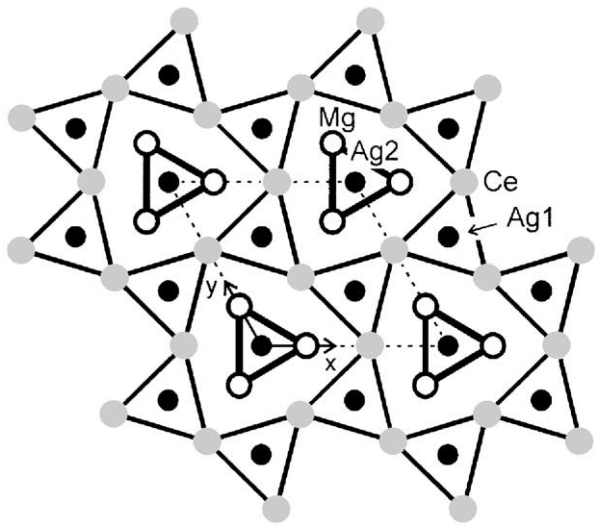

FIG. 1. Projection of the CeAgMg structure onto the *xy* plane. All atoms lie on mirror planes at $z = 0$ (thin lines) and $z = \frac{1}{2}$ (thick lines). The silver-centered trigonal prisms are emphasized.

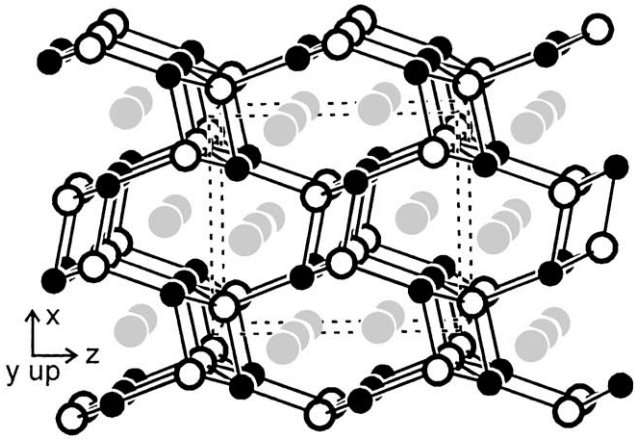

FIG. 2. View of the EuAuMg structure approximately along the *y* axis. The europium, gold, and magnesium atoms are drawn as gray, black, and open circles, respectively. The three-dimensional [AuMg] network is emphasized.

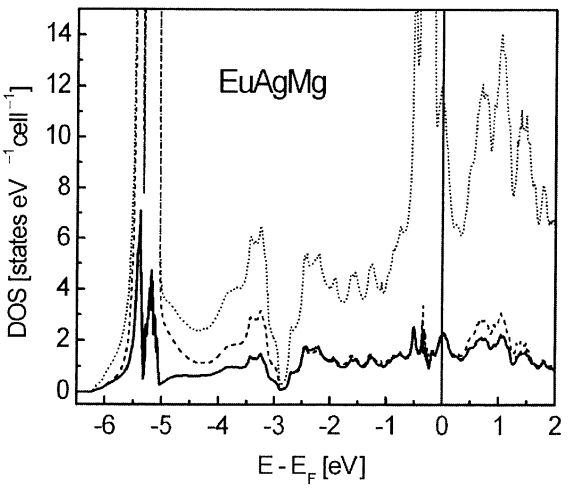

FIG. 4. Electronic density of states (DOS) of EuAgMg. Dotted line, total DOS; dashed line, silver contribution; solid line, magnesium contribution. The energy zero is taken at the Fermi level.

distances within these Au_3Mg_3 hexagons are 284 and 294 pm, slightly longer than the sum of Pauling's single-bond radii of 270 pm for gold and magnesium (21). Due to the strong puckering, we observe even the shortest Au–Mg distances (284 pm) between the layers (Fig. 3). Along with the puckering we observe the formation of Au_2Mg_2 rectangles between the layers. These Au_2Mg_2 rectangles tilt to move the more electronegative gold atoms away from each other (22, 23). Consequently, the magnesium atoms come closer together at a Mg–Mg distance of 327 pm, slightly longer than that in *hcp* magnesium (320 pm) (24). Already, the comparison of these Mg–Mg distances implies the formation of weak Mg–Mg bonds in EuAuMg.

Figure 4 shows the total electronic density of states (DOS, dotted line) and the contributions of silver (dashed line) and magnesium (solid line) of EuAgMg. The band structure calculation confirms the metallic properties as found experimentally by the electrical conductivity measurements (see Fig. 11). At the Fermi level, the DOS of EuAgMg is roughly composed of 60% europium states and each 20% states from magnesium and silver. From the spin-polarized calculation we obtain a magnetic moment of 7.99 μ_B, in excellent agreement with the magnetic measurements and confirming the divalent state of europium. The sharp peaks located at -5.5 and -0.5 eV originate from localized Ag 4*d* and Eu 4*f* orbitals, respectively. A particular feature of the EuAgMg DOS is the substantial occupation of magnesium states, which may not be expected from electronegativity reasons. As seen from the solid line in Fig. 4, the Mg 3*s* states are around -5.5 eV and mix with the Ag 4*d* states. The Mg 3*p* states extend from -5 eV to the Fermi level and play about the same part to the DOS as the silver states, whereas the europium contribution is small in this energy range. Thus, the silver and magnesium states form a valence band that is not much different as those from isostructural compounds with more electronegative elements instead of magnesium (25). From this point of view it is reasonable to

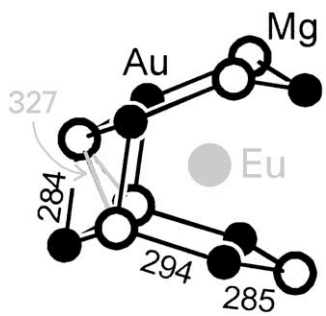

FIG. 3. Coordination of the europium atoms in EuAuMg. Relevant interatomic distances within the [AuMg] network are indicated.

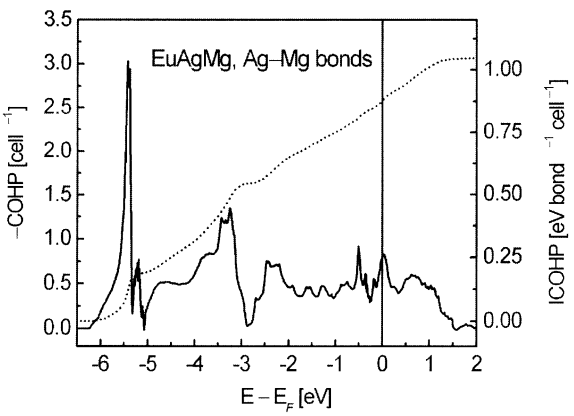

FIG. 5. COHP diagram of the Ag–Mg bonds in EuAgMg. Dotted line, COHP integration.

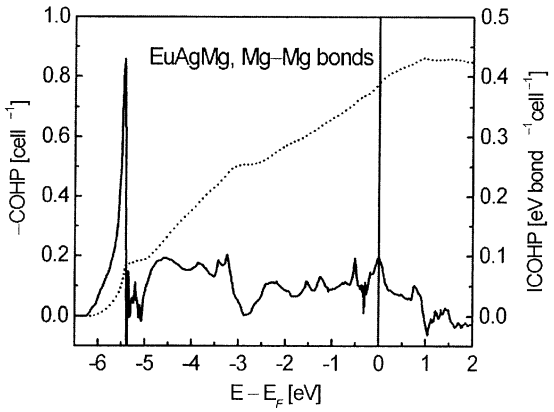

FIG. 6. COHP diagram of the Mg–Mg bonds in EuAgMg. Dotted line, COHP integration.

describe EuAgMg with a covalent $[AgMg]^{\delta-}$ polyanionic network, separated and charge-balanced by positively polarized europium atoms. This view is supported by the COHP diagram of the Ag–Mg bonds shown in Fig. 5.

For clarity, the slightly different contributions from each of the four bonds are merged. Solely bonding states are occupied, but the number of valence electrons is not sufficient to fill them completely. As we have reported for comparable compounds (26), even 18 electrons per formula unit would fill all bonding states. The idealized formula splitting $Eu^{2+}[AgMg]^{2-}$ gives 15 electrons within the polyanion and consequently the bonding levels can only be partially filled. From the COHP diagram in Fig. 5 we see that maximum bonding would be reached if the states up to ~ 1.6 eV would be occupied. If we count the number of states in the corresponding DOS (Fig. 4) up to this energy, we find about three additional electrons per formula unit would be necessary. This shows clearly that the bonding picture as derived for compounds with more electronegative elements than magnesium remains valid for EuAgMg and the related *LnT*Mg compounds.

The Mg–Mg distances within the [AgMg] network of 335 pm are only slightly longer than the average Mg–Mg distances of 320 pm in *hcp* magnesium, which may indicate Mg–Mg bonding. Figure 6 shows the Mg–Mg COHP diagram for EuAgMg. Rather weak bonding interactions discern up to the Fermi level. However, the integration of the COHP gives a Mg–Mg bond energy of ~ 0.4 eV/bond. This is at least 60% of the energy we obtain by the same calculation method for one Mg–Mg bond in *hcp* magnesium. From this we conclude that the contacts between the magnesium atoms contribute perceptible to the stability of EuAgMg.

Despite the same covalent radii of silver and gold (134 pm, (21)), we find longer Ag–Mg distances of 291–302 pm in EuAgMg than Au–Mg distances of 284–294 pm in EuAuMg. This may have electronic reasons, and also relativistic effects might account for this situation (27). To show this effect, we have calculated the DOS of EuAuMg with and without regard to the relativistic terms. As seen from Fig. 7, the gold 5*d*-orbitals are strongly affected; their energy increases by more than 1 eV and they become broadened. At the same time, the 6*s* energy decreases and both effects together lead to stronger 6*s*–5*d* hybridization. Consequently, the gold 5*d* orbitals can contribute more to Au–Mg bonding than the silver 4*d* orbitals do for Ag–Mg bonding.

Magnetic and Electric Properties

The temperature dependence of the magnetic suscetibility of LaAgMg is displayed in Fig. 8. Down to about 50 K, the susceptibility is nearly independent of temperature with

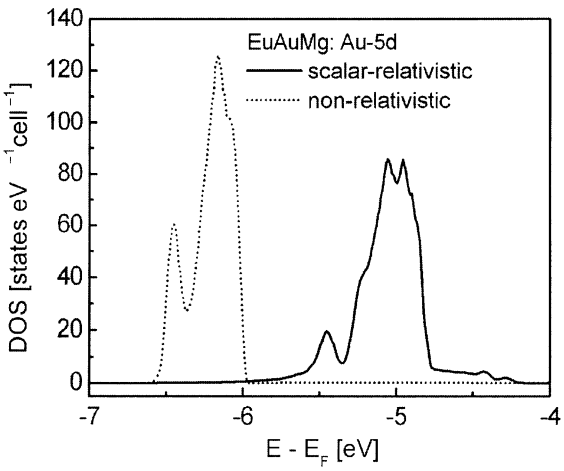

FIG. 7. Au 5*d* DOS of EuAuMg, calculated by using relativistic terms (solid line) and by neglecting them (dotted line).

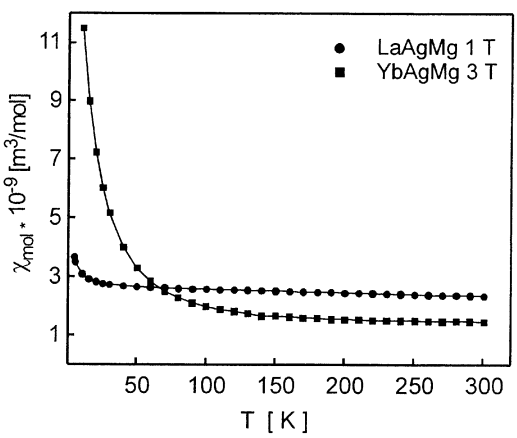

FIG. 8. Temperature dependence of the magnetic susceptibility of LaAgMg and YbAgMg, measured at field strengths of 1 and 3 T, respectively.

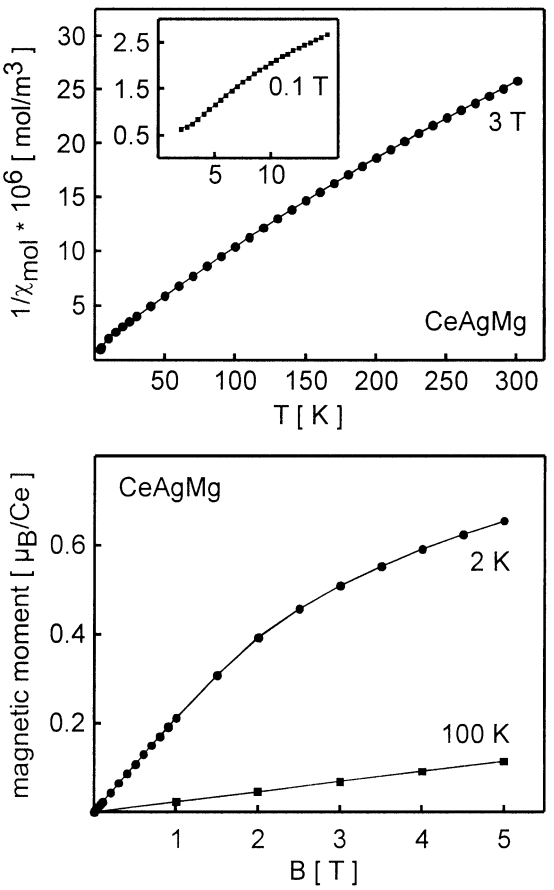

FIG. 9. Temperature dependence of the inverse magnetic susceptibility of CeAgMg (upper part) at 3 T. The low-temperature behavior is shown in the insert. In the lower part the magnetization isotherms at 2 and 100 K are presented.

a room temperature value of $2.4(1)\cdot 10^{-9}$ m^3/mol. This is compatible with Pauli paramagnetism in agreement with the metallic behavior discussed below. The small increase of the susceptibility at low temperature may be attributed to trace amounts of paramagnetic impurities.

In Fig. 9 we present the inverse susceptibility of CeAgMg as a function of temperature. CeAgMg remains paramagnetic down to 2 K. No magnetic ordering is evident in this temperature range. A small convex curvature is observed for the $1/\chi$ vs T plot, indicating a temperature-independent contribution to the total susceptibility. We have therefore fit the experimental data to a modified Curie–Weiss expression, $\chi = \chi_0 + C/(T - \Theta)$, resulting in an experimental magnetic moment of $\mu_{exp} = 2.52(2)\ \mu_B$/Ce, a paramagnetic Curie temperature (Weiss constant) of $\Theta = -13(1)$ K and a temperature-independent term, $\chi_0 = 2.3(1)\times 10^{-9}$ m^3/mol. The experimental magnetic moment is in good agreement with the free ion value of $\mu_{eff} = 2.54\ \mu_B$/Ce. This magnetic behavior is consistent with trivalent cerium, in agreement with the course of the cell volumes (8). The stronger deviation of the inverse susceptibilitiy from Curie–Weiss behavior below 50 K may be attributed to crystal field splitting of the $J = 5/2$ ground state of the Ce^{3+} ions. Crystal field effects may also account for the broad shoulder in the electric resistivity (see Fig. 11).

The magnetization data are plotted in Fig. 9. At 100 K the magnetization isotherm is linear, as expected for a paramagnetic material. At 5 T the magnetization is very small, i.e., 0.11 μ_B/Ce. Some curvature is observed for the magnetization curve at 2 K. The magnetization value of 0.66 μ_B/Ce at 5 T, however, is significantly smaller than the theoretical saturation magnetization for Ce^{3+} of 2.14 μ_B/Ce. The slight increase of the magnetization at 2 K may be attributed to a partial parallel spin alignment. The reduced value also expresses the crystal field splitting effects on the $J = \frac{5}{2}$ ground state. Very similar magnetic behavior has recently been observed for isotypic CePdMg (3) and for the stannide $Ce_3Pd_4Sn_6$ (28).

EuAgMg and EuAuMg show Curie–Weiss behavior (Figs. 10a and 10b) above 60 K with experimental magnetic moments of 7.99(5) μ_B/Eu for the silver and 7.80(5) μ_B/Eu for the gold compound, close to the free ion value of 7.94 μ_B for Eu^{2+}. The low-temperature behavior is shown in the inserts. The vanishing $1/\chi$ behavior is indicative of ferromagnetic ordering. The exact Curie temperatures were determined from kink-point measurements (Figs. 10c and 10d). We have therefore measured the susceptibility in a very low external field at 0.002 T in the zero-field-cooling (zfc) and field-cooling (fc) mode. The derivatives $d\chi/dT$ of the field-cooling measurements (inserts of 10c and 10d) resulted in Curie temperatures of $T_C = 22.0(3)$ K and $T_C = 36.5(5)$ K for EuAgMg and EuAuMg, respectively.

The observed difference between the magnetization curves taken upon cooling the specimens in zero (ZFC, zero-field-cooling) and non-zero (FC, field-cooling) magnetic field may be attributed to domain effects. The field-cooling measurements yield considerably higher values of the magnetization in the ordered region because it corresponds to probing of the response to the magnetic field of a nearly single-domain sample.

The magnetization data are plotted in Figs. 10e and 10f. Both compounds show saturation at 2 K and 5 T with saturation magnetizations of $\mu_{sm(exp)} = 7.1(1)\ \mu_B$/Eu for EuAgMg and $\mu_{sm(exp)} = 7.3(1)\ \mu_B$/Eu for EuAuMg, slightly higher than the theoretical value of $\mu_{sm(calc)} = 7.0\ \mu_B$ according to $\mu_{sm(calc)} = gJ\ \mu_B$ (29). This is similar to the magnetic behavior observed recently for isotypic EuAuCd (6) and other equiatomic EuTX intermetallics (25, 30). In view of the very small hysteresis and coercivity, both compounds may be classified as soft ferromagnets.

The susceptibilities of YbAgMg were almost identical at 3 and 5 T, indicating very minor amounts of ferromagnetic impurities. We therefore present the 3 T data in Fig. 8. At room temperature, the susceptibility is $1.5(1)\times 10^{-9}$ m^3/mol

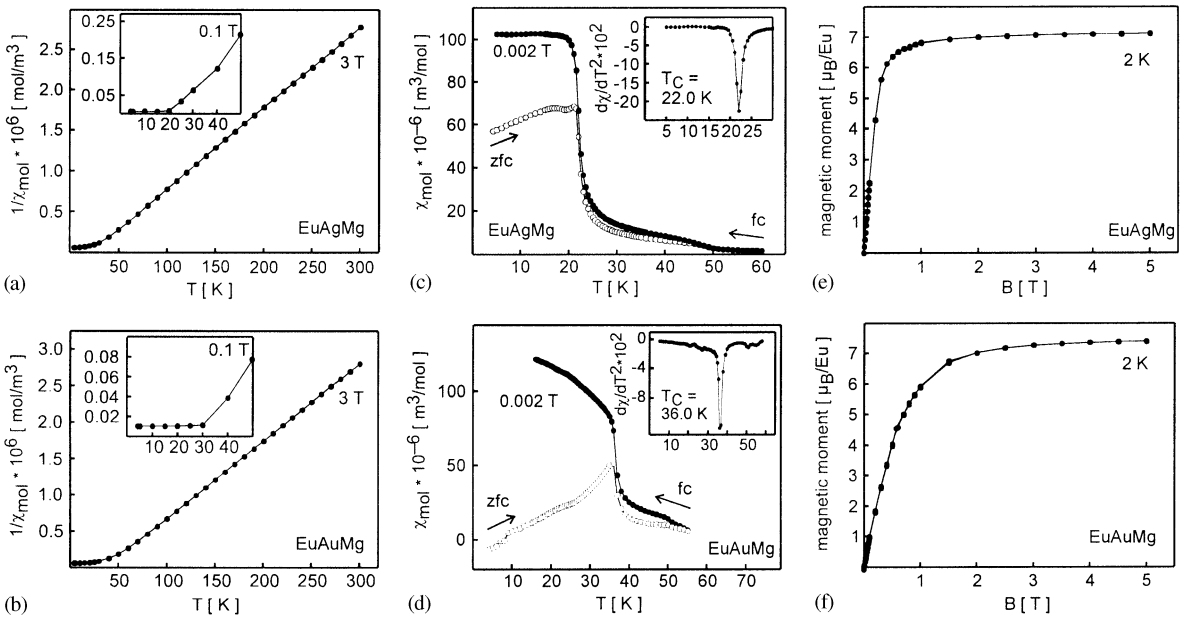

FIG. 10. Magnetic properties of EuAgMg and EuAuMg: (a) and (b), temperature dependence of the inverse magnetic susceptibilities with the low-temperature behavior presented in the inserts; (c) and (d), low-temperature susceptibilities measured in the zero-field-cooling (zfc) and field-cooling (fc) mode (kink-point measurements); the Curie temperatures of 22.0(3) K (EuAgMg) and 36.0(3) K (EuAuMg) were obtained from the derivatives $d\chi/dT$ (inserts of (c) and (d)); (e) and (f) magnetization isotherms at 2 K.

and it increases to $11.5(1) \times 10^{-9}$ m^3/mol at 4 K. The increase below about 100 K may be attributed to a paramagnetic part of the total susceptibility. We have therefore fitted the experimental data to a modified Curie–Weiss expression, resulting in a temperature-independent term, $\chi_0 = 1.3(1) \times 10^{-9}$ m^3/mol, a Weiss constant of 33(1) K, and a small experimental magnetic moment of $\mu_{exp} = 0.17(1)\ \mu_B$/Yb. This behavior is typically observed for equiatomic YbTX intermetallics with divalent ytterbium (nonmagnetic ground state). For details we refer to a recent review (31).

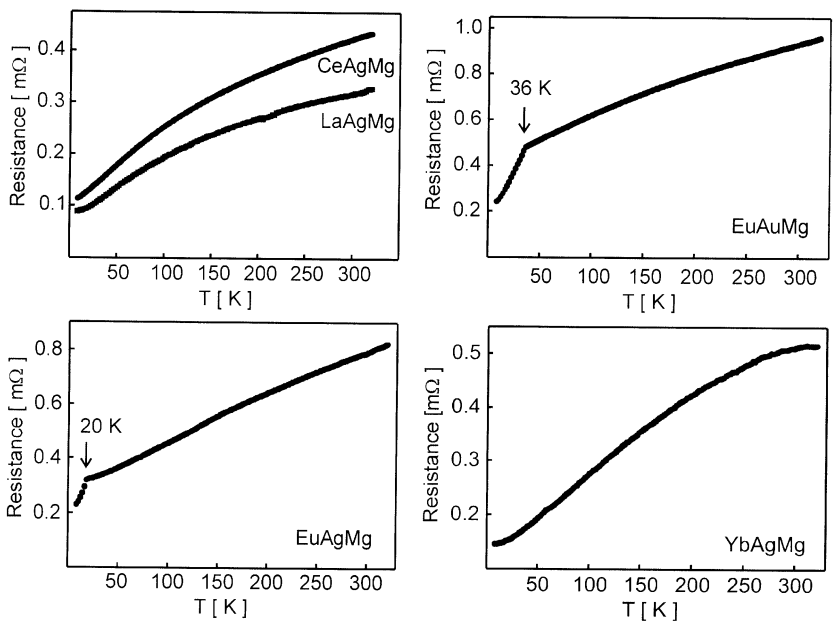

FIG. 11. Temperature dependence of the electrical resistance of REAgMg (RE = La, Ce, Eu, Yb) and EuAuMg.

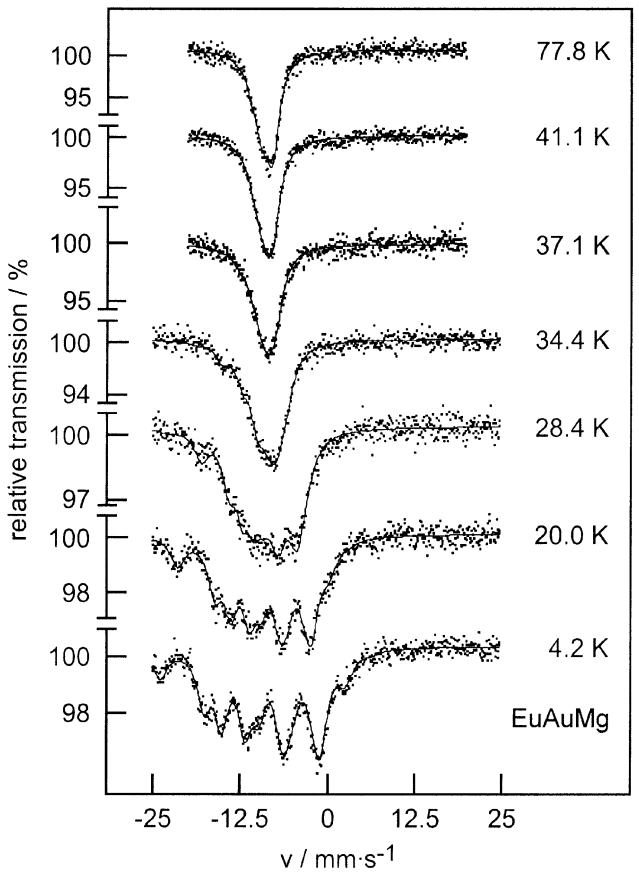

FIG. 12. Temperature-dependent ^{151}Eu Mössbauer spectra of EuAuMg. Solid curves denote simulations (see text and Table 1).

The temperature dependence of the electrical resistance of all compounds is displayed in Fig. 11. The resistance decreases with decreasing temperature, indicating metallic behavior for LaAgMg, CeAgMg, EuAgMg, EuAuMg, and YbAgMg, in agreement with the electronic structure calculations. At about 20 and 36 K the resistance curves of EuAgMg and EuAuMg show discontinuities that are attributed to freezing of spin-disorder scattering below the Curie temperature. The transition temperatures agree with those determined from the susceptibility measurements.

^{151}Eu Mössbauer Spectroscopy

The ^{151}Eu Mössbauer spectra of EuAgMg and EuAuMg at various temperatures are presented in Figs. 12 and 13 together with transmission integral fits. The corresponding fitting parameters are listed in Table 1. The fitting parameters for the 26 and 7.6 K measurements of EuAgMg (not shown in Fig. 13) are also listed in that Table. The spectra show no signal around 0 mm/s, indicating purely divalent europium in EuAgMg and EuAuMg. The 78 K spectra show single signals at $\delta = -9.00(4)$ mm/s (EuAgMg) and $\delta = -8.72(8)$ mm/s (EuAuMg), subject to quadrupole splitting of 8.5(7) mm/s (EuAgMg) and 16.8(5) mm/s. The single signals are in agreement with the single europium site observed in the TiNiSi-type structures of EuAgMg and EuAuMg (5, 8). The experimentally determined linewidths are close to the usual linewidth of 2.3 mm/s of europium. For the spectra recorded in the paramagnetic range a small asymmetry parameter was included in all fits (see Table 1).

In a recent systematic investigation of the ^{151}Eu isomer shifts in EuTX (T = transition metal, X = In, Ga, Si, Ge, Sn, P, As, Sb, Bi) compounds we revealed a linear correlation with the electron count (30). The isomer shift decreases with increasing electron count. Also, the recently reported compound EuAuCd ($\delta = -9.33(5)$ mm/s at 78 K) (6) and the two compounds reported herein with a total of 15 valence electrons per formula unit perfectly fit in this correlation.

The onset of magnetic ordering is detected around 22 K for the silver and around 37 K for the gold compound. The magnetic ordering temperatures are in good agreement with the Curie temperatures determined from the susceptibility data. Slightly below the ordering temperature the static magnetic flux density at the europium nuclei is small

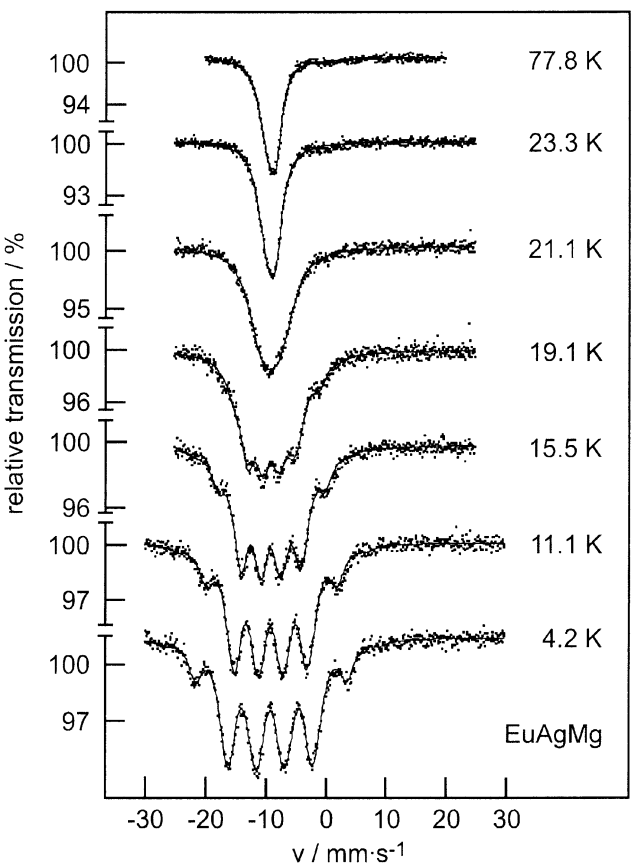

FIG. 13. Temperature-dependent ^{151}Eu Mössbauer spectra of EuAgMg. Solid curves denote simulations (see text and Table 1).

TABLE 1

Fitting Parameters of ^{151}Eu Mössbauer Measurements on EuAgMg and EuAuMg (Numbers in Parentheses Represent the Statistical Errors. Parameters without Parentheses Were Kept Fixed during the Fitting Procedure)

T (K)	δ (mm s^{-1})	Γ (mm s^{-1})	ΔE_Q (mm s^{-1})	η	B (T)
		EuAgMg			
77.8	− 9.00(4)	2.1(1)	8.5(7)	0.2(1)	0
26	− 8.98(3)	2.2(1)	8.5(7)	0.3(1)	0
23.3	− 9.00(4)	2.3(2)	8.5(7)	0.4(1)	0
21.1	− 8.9(1)	3.5(6)	− 1.0(5)	0	4.6(6)
19.1	− 8.7(2)	2.8(3)	− 1.8(9)	0	9.8(2)
15.5	− 8.86(5)	2.5(1)	− 0.5(3)	0	12.2(1)
11.1	− 8.84(5)	2.4(1)	− 0.5(3)	0	15.0(1)
7.6	− 8.85(4)	2.4(1)	− 0.5(3)	0	16.2(1)
4.2	− 8.88(4)	2.4(1)	− 0.5(3)	0	17.4(1)
		EuAuMg			
77.8	− 8.72(8)	2.1 (2)	10.3(5)	0.2(1)	0
41.1	− 8.70(7)	2.3 (3)	9.3(9)	0.2(1)	0
37.1	− 8.7(1)	2.3	12(2)	0	1.8(8)
34.4	− 8.7(1)	2.3 (4)	11(2)	0	5.4(4)
28.4	− 8.7(1)	2.3	9(1)	0	10.3(3)
20	− 8.6(1)	2.3 (3)	9.1(9)	0	15.0(3)
4.2	− 8.64(8)	2.3 (2)	9.3(8)	0	18.3(2)

Note. δ, isomer shift; Γ, linewidth; ΔE_Q, electric quadrupole interaction; η, asymmetry parameter; B, magnetic hyperfine field.

and the uncertainty of the absolute value is relatively high. The flux density then increases with decreasing temperature. Full magnetic hyperfine field splitting is observed at 4.2 K with static magnetic flux densities of 17.4(1) T (EuAgMg) and 18.3(2) T (EuAuMg), as frequently observed in related EuTX compounds (25). The temperature dependence of the internal magnetic hyperfine field at the europium nuclei approximately follows the Brillouin function for $J = 7/2$ (Figs. 14 and 15) for both compounds.

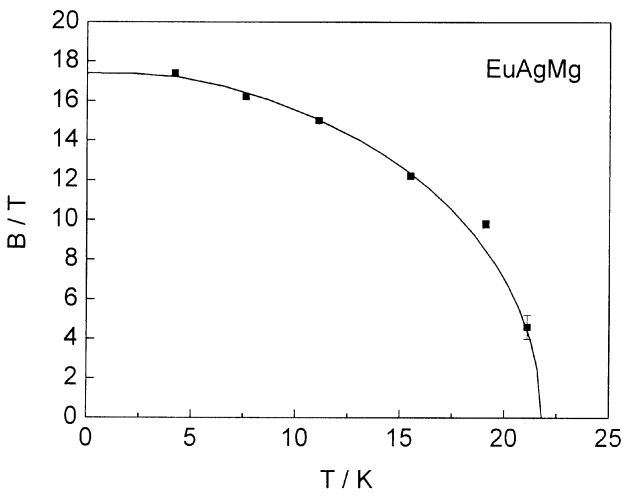

FIG. 14. Temperature dependence of the internal magnetic hyperfine field at the europium nuclei in EuAgMg. It approximately follows the Brillouin function for $J = \frac{7}{2}$.

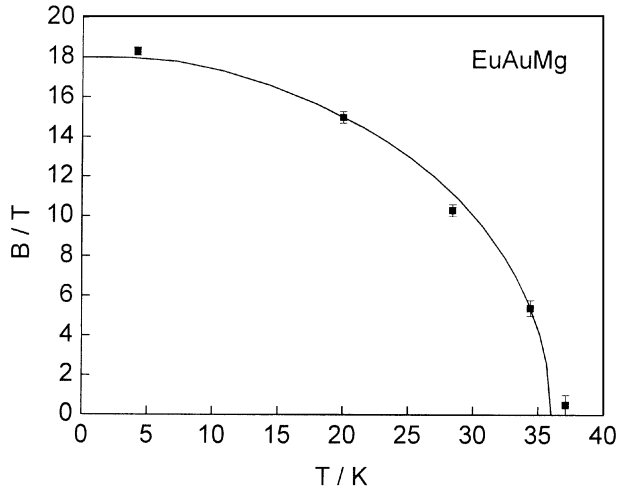

FIG. 15. Temperature dependence of the internal magnetic hyperfine field at the europium nuclei in EuAuMg. It approximately follows the Brillouin function for $J = \frac{7}{2}$.

In EuAgMg the onset of magnetic ordering is associated with a drastic reduction in the magnitude of the electrical field gradient (EFG) parameter used to optimize the least-squares fit to the data, suggesting that the angle defining the EFG principle axis is close to the magic angle. This behavior is similar to that in EuPdIn (32) and $Eu_2Si_5N_8$ (33). No change is observed for the electric field gradient in EuAuMg, indicating that the hyperfine field and the EFG are almost parallel.

CONCLUSIONS

The ternary intermetallic magnesium compounds REAgMg (RE = La, Ce, Eu, Yb) and EuAuMg have been investigated by magnetic susceptibility, electrical resistance, and ^{151}Eu Mössbauer spectroscopic measurements. Chemical bonding in EuAgMg and isotypic EuAuMg was studied by TB-LMTO-ASA band structure calculations. LaAgMg and YbAgMg are Pauli paramagnetic while CeAgMg displays Curie–Weiss behavior (trivalent cerium) but no magnetic ordering down to 2 K. EuAgMg and EuAuMg order ferromagnetically at the relatively high Curie temperatures of $T_C = 22.0(3)$ and 36.5(5) K, respectively. Full magnetic hyperfine field splitting is detected at 4.2 K in the ^{151}Eu Mössbauer spectra.

ACKNOWLEDGMENTS

We are grateful to the Degussa-Hüls AG for a generous gift of gold and silver wire. This work was financially supported by the Fonds der Chemischen Industrie and the Deutsche Forschungsgemeinschaft.

REFERENCES

1. A. Iandelli, *J. Alloys Compd.* **182,** 87 (1992).
2. A. Iandelli, *J. Alloys Compd.* **203,** 137 (1994).
3. C. Geibel, U. Klinger, M. Weiden, B. Buschinger, and F. Steglich, *Physica B* **237–238,** 202 (1997).
4. A. I. Horechyy, V. V. Pavlyuk, and O. I. Bodak, *Pol. J. Chem.* **73,** 1681 (1999).
5. R. Pöttgen, R.-D. Hoffmann, J. Renger, U. Ch. Rodewald, and M. H. Möller, *Z. Anorg. Allg. Chem.* **626,** 2257 (2000).
6. R. Mishra, R. Pöttgen, R.-D. Hoffmann, D. Kaczorowski, H. Piotrowski, P. Mayer, C. Rosenhahn, and B. D. Mosel, *Z. Anorg. Allg. Chem.* **627,** 1283 (2001).
7. R.-D. Hoffmann, Th. Fickenscher, R. Pöttgen, C. Felser, K. Łątka, and R. Kmieć, *Solid State Sci.*, in press.
8. Th. Fickenscher and R. Pöttgen, *J. Solid State Chem.* **161,** 67 (2001).
9. P. I. Krypyakevich, V. Ya. Markiv, and E. V. Melnyk, *Dopov. Akad. Nauk. Ukr. RSR, Ser. A* 750 (1967).
10. A. E. Dwight, M. H. Mueller, R. A. Conner, Jr., J. W. Downey, and H. Knott, *Trans. Met. Soc. AIME* **242,** 2075 (1968).
11. M. F. Zumdick, R.-D. Hoffmann, and R. Pöttgen, *Z. Naturforsch. B* **54,** 45 (1999).
12. C. B. Shoemaker and D. P. Shoemaker, *Acta Crystallogr.* **18,** 900 (1965).
13. K. Yvon, W. Jeitschko, and E. Parthé, *J. Appl. Crystallogr.* **10,** 73 (1977).
14. O. K. Andersen and O. Jepsen, Tight-Binding LMTO Vers. 47, Max-Planck-Institut für Festkörperforschung, Stuttgart, 1994.
15. O. Jepsen, M. Snob, and O. K. Andersen, "Linearized Band Structure Methods and its Applications," Springer Lecture Notes. Springer-Verlag, Berlin, 1987.
16. H. L. Skriver, "The LMTO Method." Springer-Verlag, Berlin, 1984.
17. O. K. Andersen and O. Jepsen, *Solid State Commun.* **9,** 1763 (1971).
18. W. R. L. Lambrecht and O. K. Andersen, *Phys. Rev. B* **34,** 2439 (1986).
19. U. Barth and L. Hedin, *J. Phys. C: Solid State Phys.* **5,** 1629 (1972).
20. R. Dronskowski and P. Blöchl, *J. Phys. Chem.* **97,** 8617 (1993).
21. L. Pauling, "The Nature of the Chemical Bond and the Structures of Molecules and Crystals." Cornell Univ. Press, Ithaca, NY, 1960.
22. G. Nuspl, K. Polborn, J. Evers, G. A. Landrum, and R. Hoffmann, *Inorg. Chem.* **35,** 6922 (1996).
23. G. A. Landrum, R. Hoffmann, J. Evers, and H. Boysen, *Inorg. Chem.* **37,** 5754 (1998).
24. J. Donohue, "The Structures of the Elements." Wiley, New York, 1974.
25. R. Pöttgen and D. Johrendt, *Chem. Mater.* **12,** 875 (2000).
26. D. Johrendt and A. Mewis, *Z. Naturforsch. B* **51,** 655, (1996).
27. H. Schmidbaur, *Gold Bull.* **11,** 23 (1990).
28. D. Niepmann, R. Pöttgen, B. Künnen, G. Kotzyba, and B. D. Mosel, *Chem. Mater.* **12,** 533 (2000).
29. H. Lueken, "Magnetochemie." Teubner, Stuttgart, 1999.
30. R. Müllmann, U. Ernet, B. D. Mosel, H. Eckert, R. K. Kremer, R.-D. Hoffmann, and R. Pöttgen, *J. Mater. Chem.* **11,** 1133 (2001).
31. R. Pöttgen, D. Johrendt, and D. Kußmann, *in* "Handbook on the Chemistry and Physics of Rare Earths" (K. A. Gschneidner, Jr., and L. Eyring, Eds.), Elsevier Science, Amsterdam, Vol. 32, Chap. 207. 2001.
32. R. Müllmann, B. D. Mosel, H. Eckert, G. Kotzyba, and R. Pöttgen, *J. Solid State Chem.* **137,** 174 (1998).
33. H. A. Höppe, H. Trill, B. D. Mosel, H. Eckert, G. Kotzyba, R. Pöttgen, and W. Schnick, *J. Phys. Chem. Solids*, in press.